Geophysical Research Letters

RESEARCH LETTER
10.1029/2019GL083025

Peatland Volume Mapping Over Resistive Substrates With Airborne Electromagnetic Technology

Sonia Silvestri[1,2], Craig W. Christensen[3], Asgeir O. K. Lysdahl[3], Helgard Anschütz[3], Andreas A. Pfaffhuber[3], and Andrea Viezzoli[4]

[1]Department TESAF, Universitá di Padova, Padova, Italy, [2]Nicholas School of the Environment, Duke University, Durham, NC, USA, [3]Norwegian Geotechnical Institute, Oslo, Norway, [4]Aarhus Geophysics, Aarhus, Denmark

Key Points:
- Airborne electromagnetic can be successfully used to estimate peat thickness and extension even over resistive substrata
- The 3-D geometry and volume of selected Norwegian bogs were determined
- The carbon pool is determined by combining the 3-D peatland model with the soil organic carbon content retrieved from field/laboratory analyses

Supporting Information:
- Supporting Information S1
- Figure S1
- Figure S2
- Figure S3
- Figure S4
- Figure S5
- Figure S6

Correspondence to:
S. Silvestri,
sonia.silvestri@duke.edu

Citation:
Silvestri, S., Christensen, C. W., Lysdahl, A. O. K., Anschütz, H., Pfaffhuber, A. A., & Viezzoli, A. (2019). Peatland volume mapping over resistive substrates with airborne electromagnetic technology. *Geophysical Research Letters*, *46*, 6459–6468. https://doi.org/10.1029/2019GL083025

Received 4 APR 2019
Accepted 28 MAY 2019
Accepted article online 5 JUN 2019
Published online 24 JUN 2019

Abstract Despite the importance of peatlands as carbon reservoirs, a reliable methodology for the detection of peat volumes at regional scale is still missing. In this study we explore for the first time the use of airborne electromagnetic (AEM) to detect and quantify peat thickness and extension of two bogs located in Norway, where peat lays over resistive bedrock. Our results show that when calibrated using a small amount of field measurements, AEM can successfully detect peat volume even in less ideal conditions, that is, relatively resistive peat over resistive substrata. We expect the performance of AEM to increase significantly in presence of a conductive substratum without need of calibration with field data. The organic carbon content retrieved from field surveys and laboratory analyses combined with the 3-D model of the peat extracted from AEM allowed us to quantify the total organic carbon of the selected bogs, hence assessing the carbon pool.

Plain Language Summary Wetlands hide a secret. We may know them for their beauty and valuable ecological services, but the real treasure of these environments is hidden underground. It is the carbon pool that these ecosystems build every day, inch by inch, subtracting carbon dioxide from the atmosphere and storing it underground. This process forms a dark soil extremely rich in organic matter that we call "peat." Peatlands around the world store almost the same amount of carbon that is present in the atmosphere. The problem is that, spoiling peat, the carbon is released as carbon dioxide and we have less carbon stored underground and more greenhouse gasses in atmosphere. The first step we should take in order to protect peatlands is to find effective methodologies to map them. In this study, we use an instrument carried by a helicopter that allows us to explore under the soil surface. We show for the first time that this technology, called airborne electromagnetics, can be used to quantify the peat stored underground in boreal peatlands. Thanks to this methodology, we can now map large areas and calculate the amount of carbon stored in peatlands, which is the first step toward implementing better conservation policies.

1. Introduction

The conservation of peatlands is one of the main measures indicated by the Intergovernmental Panel on Climate Change to mitigate climate change (Intergovernmental Panel on Climate Change, 2014). Peatlands, in fact, are extraordinary deposits of organic carbon, and their protection is of key importance in order to avoid emissions due to degradation (Ballhorn et al., 2009; Page et al., 2002; Turetsky et al., 2015). Peat is a mixture of organic material produced by wetland plants and accumulated in the soil when continuously or cyclically anaerobic conditions are present for long periods. Peatlands can be found over a wide range of latitudes, in tropical, to temperate, to (sub)polar climates. It is estimated that globally about 2%–3% of the land surface is covered by peatlands, storing 500–700 Gt of carbon, that is, likely exceeding the carbon content of the terrestrial vegetation globally (~560 GtC) and almost equaling the size estimated for the atmosphere carbon pool (~850 GtC; Turetsky et al., 2015). Unfortunately, the uncertainty affecting our best estimates of the size of the peatland carbon pool is significant, mainly due to inaccurate estimates of their volume and ecological characteristics (Joosten, 2010).

Despite the urgent need for a precise quantification of peat deposits from the local to the regional scale, the number of studies dealing with this topic is extremely limited. Remote sensing (RS) has been employed for this task, making use of satellite and airborne laser instruments and radar sensors (e.g., Ballhorn et al., 2011), as well as a combination of these techniques with multispectral sensors (Draper et al., 2014; Rudiyanto et al.,

2018) and mathematical models (Jaenicke et al., 2008). However, classic RS does not provide direct information on the nature of the underground characteristics; hence, it has been exclusively used to provide input to approximate models of peatland thickness. A new approach is needed, making optimal use of limited field information and using remotely sensed data that allow the detection of belowground soil characteristics.

Some ground geophysical methods have been shown to be extremely effective in detecting peat deposits, both laterally and in depth. Ground penetrating radar (GPR) has been proven to be the most reliable and precise ground geophysical method to detect peat thickness (Comas et al., 2015; Slater & Reeve, 2002; Warner et al., 1990). Ground electrical resistivity mapping has been also found successful in several applications (Boon et al., 2008; Comas et al., 2015; Elijah et al., 2012; Kowalczyk et al., 2017). Induced polarization imaging is another viable method because of the chargeability of peat (Comas & Slater, 2004; Slater & Reeve, 2002). Even though peat usually is electrically more resistive than the substrate (often clays), ground geophysical measurements have shown that there are several examples of peat over resistive unit, both in tropical environments (Comas et al., 2015) and in northern European countries (Boon et al., 2008; Kowalczyk et al., 2017). Ground geophysics, however, is usually applied to relatively small areas (order of magnitude of ~1 km^2), and it is extremely difficult to perform in flooded ecosystems like wetlands/peatlands.

Airborne electromagnetic (AEM) has the potential of contributing to mapping peat, given its ability to efficiently recover the 3-D distribution of ground resistivity not only over vast areas but also those that are difficult to access. To the best of our knowledge, AEM has never been specifically applied before for the retrieval and characterization of boreal peatlands. The closest was Puranen et al. (1999) who detected some peat deposits while mapping surficial deposits in Finland with AEM, but no analysis of its volume was undertaken. Developments of the AEM technology (better system monitoring and early time gates, e.g., Schamper et al., 2014) in the last decade have pushed it toward high-resolution near-surface deposits mapping (i.e., within the first 10 m of depth; Skurdal et al., 2018), making it potentially suitable for studying peatland characteristics, depth, and extension. In this paper, we take advantage of the presence of an AEM data set that has been acquired on Norwegian bogs, and we share our experiences in attempting peat mapping with AEM. As reported for other peatlands (Boon et al., 2008; Comas et al., 2015; Kowalczyk et al., 2017), in this case we find a resistive substrate underlying the peat. We explain how this scenario represents a challenge for AEM, showing through simulations that in the more common case of peat over a conductive substrate, AEM is more reliable and effective. We finally discuss the applicability and limits of our approach. The peat volume retrieved using AEM is used to assess the carbon pool currently available in the study site.

2. Study Site and Data Collection

The study site is located just under 200 km north of Norway's capital Oslo, near a village called Brøttum (Ringsaker; Figures 1 and S1 in the supporting information). The area is characterized by the presence of several small bogs on frequent bedrock depressions, at 300–400 m above mean sea level. Wetlands are usually covered by a thick carpet of sphangnum moss and surrounded by forested land. The peat thickness is variable, in many cases higher than 1 m as indicated by the map of wetlands that was kindly provided by NIBIO—Norwegian Institute of Bioeconomy Research. The map also shows the location of mires with weakly humified peat in the upper layer. The map (scale 1:10,000) was created by a combination of field controls and air photo interpretation, and the peat depth was measured using a simple 1-m auger. The technical accuracy of delineation was 2 to 10 m, and the minimum mapping unit was 0.2 ha. The maps were scanned in the 1990 and converted to digital format. The area is else dominated by moraine, and bedrock is composed largely of early to late pre-Cambrian sandstone and some intermittent shales and limestone. The characteristics of these geological structure is, by nature, highly spatially variable in terms of composition and structure.

An AEM survey performed July/August 2015 is available on this study site. The data set was collected as part of the InterCity Project (Norwegian Geotechnical Institute, 2015; Pfaffhuber et al., 2016) and was kindly provided by the National Norwegian Railroad Authorities (BaneNOR). The survey had used the SkyTEM 304, a time domain electromagnetic system suspended from a helicopter that flies at less than one hundred meters above ground (the AEM system itself is kept at approximately 30 m above ground). The transmitter and the coils where the current circulates are mounted on an octagonal loop composed of lightweight composite

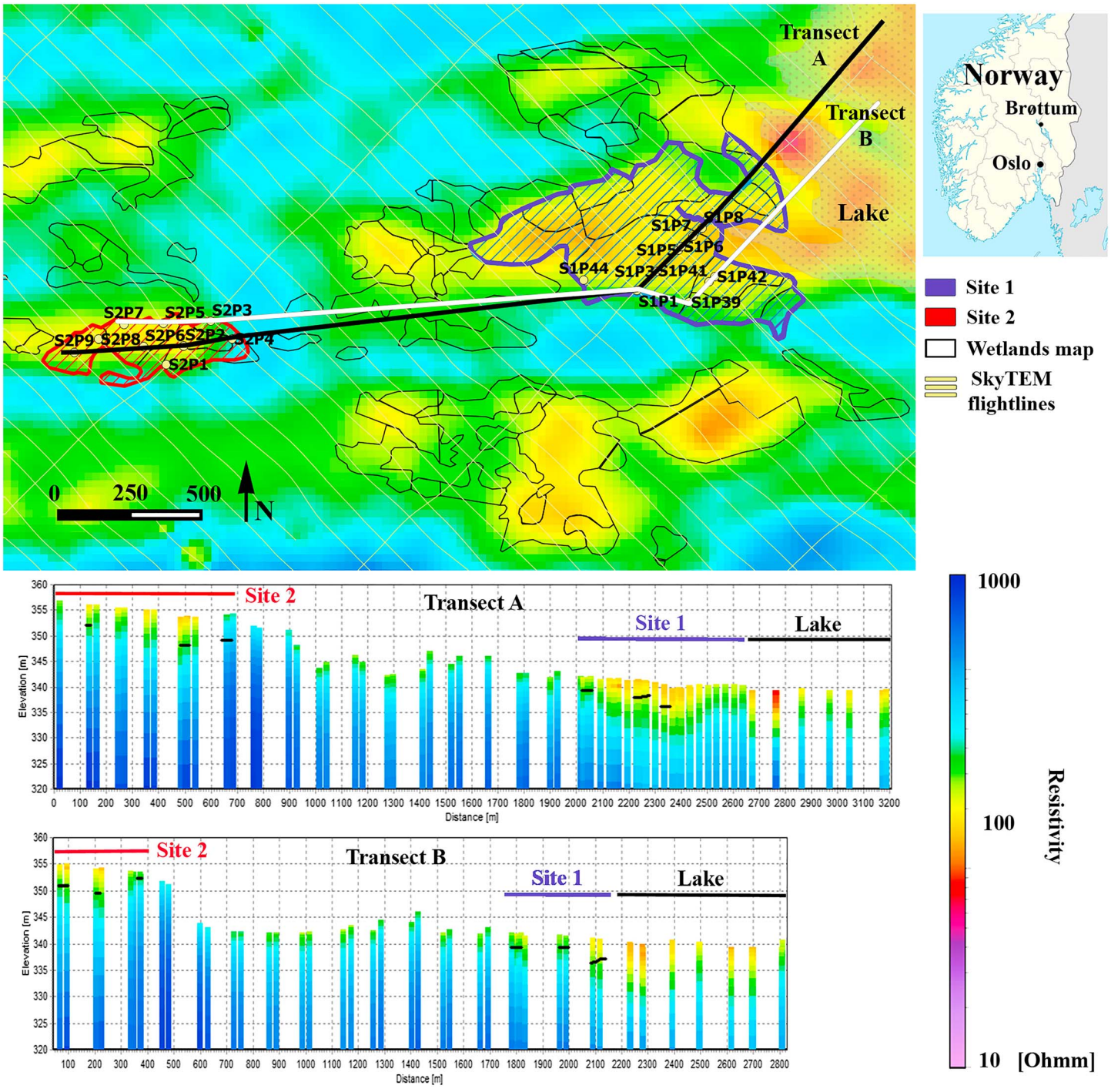

Figure 1. (top panel) Average resistivity map obtained for the interval 0–2 m of depth with the two study sites crossed by Transect A (black line) and Transect B (white line). (middle and bottom panels) Vertically electrical resistivity of the soundings recorded by the SkyTEM sensor along Transect A and Transect B. The black short segments indicate the elevation of the peat bottom recorded in the field.

tubes. In the transmitter loop a strong current is ramped to about 100 amperes and then switched off very rapidly (within 10^{-5}–10^{-4} s). This impulse creates a strong magnetic field, which in turn induces eddy currents in the ground, which decay and penetrate deeper with time. A receiver located on the same frame records the decay of the secondary field dB/dt, which, in turn, carries the information about the electrical resistivity of the underground materials. After elaborate data processing, inversion modeling provides a 3-D resistivity model that explains the measured decays within chosen uncertainty (section 3).

The peat sampling field survey was performed along the SkyTEM flight lines. Two bogs were selected and are visible in Figure 1 (for detailed visualization, see Figure S1 in the supporting information). We selected these two sites because, based on the indication given by the NIBIO's map, the peat thickness was more than 1 m. Moreover they were easily accessible. Site 1 has an area of about 36 ha, while Site 2 is smaller with an area of 9 ha.

The field sampling survey was performed between 20 and 26 August 2017. In the field, a set of measurements were carried out in order to (1) measure the thickness of the peat layer and (2) collect samples of peat in several points located along the SkyTEM flight lines. A total of 19 sampling locations were selected along the SkyTEM flight lines and located in the field using a DGPS Trimble GeoXH 3.5G. The coring activity was performed using a peat corer with an auger for wet/waterlogged soils with diameter of 2.5 cm and length of 50 cm. Even if the use of a simple push probe would have allowed a faster survey with the collection of numerous measurements, Parry et al. (2014) shows that this method may lead to a 35% error on average of peat thickness estimation; hence, we avoided it. The soil auger was pushed into the peat using length extensions until the transition from peat to the substrate was determined, and a small sample of the substrate was collected to precisely determine the peat thickness and the type of substrate. One single replicate of coring was performed in case we reached the peat bottom. A maximum of three replicates were performed at about 2–4 m of distance one from the other in case the peat bottom was not reached with the first attempt. Despite the several attempts, in 4 out of the 19 sampling locations we were not able to reach the transition surface due to the presence of rocks or roots that prevented the perforation. In one instance, peat depth exceeded the length (8.5 m) of our auger/sampling equipment. The peat depth in the remaining 14 sampling locations (where we reached the bottom) varied between 1.41 and 5.81 m.

Peat samples of 2.5 × 50 cm were collected at each location: one sample was collected between 50 and 100 cm (shallow sample) and the second between 250 and 300 cm (deep sample, which was collected only when the peat layer was deep enough). The samples were put in plastic bags and a vacuum pump was used in order to eliminate the air inside the bags and limit the decomposition of organic matter. At the end of each day, the samples were refrigerated and kept in this condition until the laboratory analyses were performed the following week.

All samples were characterized by organic material at early stage decomposition with recognizable plant fibers. No significant change in the decomposition stage was noticed at different depths. In the locations where we reached the substrate, we were able to collect 2–3 cm of it. In most cases it was formed by clay, often mixed with gravel.

3. Materials and Methods

3.1. Laboratory Analyses

A total of 31 samples were collected at the 19 coring locations. The lab analyses were performed right after the completion of the field survey, in the week of 28 August to 4 September 2017, with the purpose of determining the dry bulk density (BD) and the soil organic matter content (SOM). The samples were put in the oven at 105 ° C for 44 hr (constant weight was obtained comparing the weight of the samples after 30 and 44 hr). The BD was calculated dividing the mass of the dry sample (g) by its volume (cm^3).

The SOM was determined performing the loss of ignition (LOI). The LOI procedure determines the amount of ash contained in samples, and subtracting it from the weight of the original samples, we determine the amount of organic matter. See the supporting information for details.

The SOM obtained with the LOI does not only include carbon, so in order to calculate the total organic carbon present in the two study sites and exclude the other organic substances, we averaged the SOM content and applied a conversion factor of 1/1.724 in line with previous studies (Nelson & Sommers, 1996). The organic carbon content by soil volume was finally calculated multiplying the organic carbon content by the BD.

3.2. Airborne Electromagnetic Data Processing

Mapping the relatively resistive peat over the more resistive basement is a difficult task for EM methods, be it airborne or ground. All the information regarding peat will be stored in the very early times of the transient,

and it is possible that, in places, there will not be enough resistivity contrast between substrate and peat to resolve the latter. Moreover, if the peat layer is very thin, it might not be resolved by AEM at all. Further details about the limits of using AEM to detect peat over a resistive substrate are included in the supporting information.

SkyTEM is a comprehensive system that collects electromagnetic data as well as navigation data, which are preprocessed and then integrated in the inversion that associates the electrical resistivity to the $d\boldsymbol{B}/d\boldsymbol{t}$ (time derivative of the secondary magnetic field) signal and hence allows to differentiate the underground geological structures. The settings of the SkyTEM system can be fine tuned prior to the survey in order to maximize the capability of the sensor to detect the target of interest. In our case, the system was setup for a purpose (geotechnical applications) other than the detection of peatlands and was selected by the owner of the data set in 2015. The specific configuration settings are summarized in Table S1 in the supporting information.

For the SkyTEM data processing, we used Aarhus Workbench which is a proprietary software developed by Aarhus GeoSoftware (2018). Please refer to the supporting information for a detailed description of the applied procedure. The wide presence of infrastructures (pipes, power lines, railways, etc.) forced us to remove from the dataset large portions of data. A digital elevation model of the area was downloaded from the Norwegian National Mapping Authority website (https://hoydedata.no/LaserInnsyn/) and provided as input in the inversion as well as the maps of railways, streets, and power lines. Based on the several corrections and deletions, and considering the location of the majority of the wetlands as well as of our two study sites, we selected a smaller area to perform the inversion (compare Figures S1 and S3 in the supporting information). Since the type of regularization chosen in the inversion plays an important role in the details of the output model, several types were tested: smooth and sharp, multilayered, and few layered (Vignoli et al., 2017) spatially constrained inversions (SCI, Viezzoli et al., 2008). The best results in terms of data misfit and correlation with the distribution of wetlands provided by the NIBIO's map were obtained with multilayered spatially constrained inversion with L2 norm, loose vertical constraints, and moderate lateral constraints. Field measurements and the NIBIO's wetland distribution map were used only to compare results and not as extra a priori input to the inversion. Results obtained with other attempted inversions are discussed in the supporting information. Moreover, in order to generalize the applicability of the suggested methodology to the case of peatlands over conductive substrates, we include in the supporting information modeling results, sensitivity analysis, and a detailed discussion.

3.3. Mapping the Peat Thickness and Uncertainty Calculation

The results obtained from the AEM data analysis were used to determine the presence and extension of peat soils within a study area of 19 km^2, both horizontally and vertically. This area surrounds the two study sites where the field surveys were performed and includes several other peatlands as reported by the NIBIO map. The resistivity of the peat-substrate interface corresponding to the field points was spatially variable. Linear methods such as using a constant threshold resistivity were therefore deemed insufficient. We used an artificial neural network (ANN) to interpret peat thickness and location and hence retrieve the interface between the peat and the substrate. Specifically, we used a supervised multilayer perceptron, a type of ANN from the Python module scikit-learn with two hidden layers. The network was trained (i.e., fitted) with the peat thicknesses recorded at the field locations during the surveys, with the network weighting parameters being optimized by the limited-memory Broyden-Fletcher-Goldfarb-Shanno solver (which is a stochastic gradient-descent algorithm). The optimization equation aimed to not only minimize the mismatch between predictions and training data but also to minimize the variance (specifically, the L2 norm) of the network weights. This second term helps prevent overfitting. The relative weight of the second term was tuned manually to the lowest possible value such that the data fit was good but no obvious prediction artifacts were present.

Given that at 5 of the 19 sampling locations we did not manage to reach the peat bottom due to the presence of roots and other materials that prevented the perforation, only the remaining 14 field locations were considered. We also added 28 points homogenously distributed across the study area with zero peat thickness. These interpretations of zero peat thickness were based on the NIBIO map and visual interpretation performed on a Sentinel-2 image. This added information was found to be fundamental in order to train the algorithm to distinguish between peatlands and nonpeatlands areas. Several ANN configurations were

considered, changing the number of SkyTEM layers used to feed the model (13, 18, and 30 layers) and introducing a variable number of points with no peat (0, 6, 14, and 28 points) located across the study area (see the supporting information for details). In order to verify the accuracy of the prediction of the ANN method, a leave-one-out cross validation analysis was used to compare the measured and the simulated thicknesses (2,000 runs). We computed the average of the residuals and the root mean square error in order to evaluate the uncertainty associated with the predictive method.

4. Results

4.1. Laboratory Analyses

The BD of samples collected at Site 1 and at Site 2 are very similar (see Figure S2a in the supporting information). The values of samples collected at Site 1 varies from a minimum BD of 0.017 g/cm^3 of point S1P7(50-100) to a maximum BD of 0.092 g/cm^3 of point S1P41(250-300). However, the large majority of samples have a BD between 0.03 and 0.07 g/cm^3. The variability is slightly smaller for samples collected at Site 2, where the minimum and the maximum BD values are 0.013 and 0.073 g/cm^3, respectively, and most samples have BD values between 0.03 and 0.06 g/cm^3. Looking at the average BD values, we notice that shallow samples collected at both sites have very similar BD values ($S1_{shlw}$ = 0.043 g/cm^3 and $S2_{shlw}$ = 0.044 g/cm^3), which are also extremely close to the average value calculated for the deep samples of Site 2 ($S2_{deep}$ = 0.041 g/cm^3). A larger average BD is instead calculated using the deep samples of Site 1, which give a BD value of 0.065 g/cm^3.

The values of the SOM content retrieved from the samples using the LOI are plotted in Figure S2b in the supporting information. As we found for the BD, also in this case the shallow samples collected at Site 1 and Site 2 and the deep samples collected at Site 2 show a similar SOM content, with average values between 95.4% and 97.4%. On the contrary, the deep samples collected at Site 1 show a lower average SOM, equal to 92.7% (e.g., it is this group of measurements that includes the lowest value, which is 82%). The overall average SOM is 95.5% with a standard deviation of only 4% (Table S2 in the supporting information).

Finally, the average organic carbon content (OCC) calculated for Site 1 is very similar to the value obtained for Site 2 (Table S2), with a total average of 55.4% if we consider all the samples together and a standard deviation of 2.3%.

The small variability of both SOM and OCC is shown in Table S3 in the supporting information where we report the average and standard deviation values calculated for 35%, 50%, 65%, and 90% of the samples randomly chosen among the 31 samples.

The OCC by Soil Volume averaged for all samples is 0.026 g/cm^3 (Table S2 in the supporting information). This value corresponds to fibric peat and is in line with the observations performed in the field (i.e., early stage of peat decomposition where recognizable plant fibers dominate).

4.2. AEM Data Analysis Results

Figure 1 shows the average resistivity map obtained for the interval 0–2 m of depth for the two selected study sites. For a more comprehensive visualization of a larger portion of the study area, see Figure S3 in the supporting information, which shows the average resistivity maps obtained for the 0–2, 2–4, 4–6, and 6–8 m depth intervals. The colors associated with a range of resistivity that goes from 10 to over 1,000 Ω·m allow the visualization of the horizontal resistivity distribution in the area. Figure 1 clearly shows a qualitative agreement between the presence of wetlands (polygons outlined in black), retrieved from NIBIO map, and a resistivity range of about 100–300 Ω·m (orange-yellow in the figure). In order to visualize its vertical distribution, we have selected Transect A (black line in Figure 1) and Transect B (white line in Figure 1), which start inside the study Site 2, cross several field points and SkyTEM soundings, intercept study Site 1, and end in the nearby lake. The vertical visualizations of the resistivity distribution corresponding to the field points confirms the correlation noted above, as we notice for the transects in Figure 1 where the direct field measurement of the elevation of the peat bottom from the cores is marked by short black segments. The soundings collected on the two wetlands show a surface layer with resistivity ranging approximately between 100 and 120 Ω·m at the top and 300–320 Ω·m at the bottom, while below the bottom of the peatland the light/dark blue denotes larger resistivity values, typical of bedrock in the area. Although

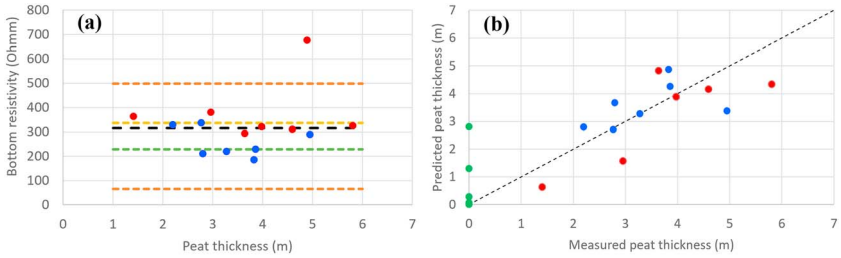

Figure 2. (a) Resistivity recorded along the SkyTEM soundings closest to the coring points and corresponding to the bottom of the peat layer. The green, black, and yellow dotted lines indicate the first, second, and third interquartile, respectively, of the resistivity values. The orange dotted lines indicate the 1.5 time interquartile range above the third quartile or below the first quartile. (b) Measured versus predicted peat thickness values; the dotted line has a 45° slope. For both panels, blue dots correspond to the points collected within Site 1, red dots correspond to points of Site 2, and green dots correspond to the 28 points with no peat.

some clay samples were collected at the bottom of a few coring locations during the field campaign, the high conductivity typical of clay is not detected by the sensor. This may be because the potential clay layer is too thin to be resolved by AEM. Soundings recorded on the lake show increasing resistivity proceeding from the top to the bottom, while soundings collected in the territory between the two bogs show surface resistivities larger than 300 Ω·m for both transects (Figure 1).

As mentioned in section 1, accurate mapping the relatively resistive (~100 Ω·m) peat over more resistive bedrock can be difficult task for electromagnetic methods, due to its lower sensitivity in resistive domains, especially when resistivity increases monotonically with depth. The positive qualitative results obtained nonetheless at the bog scale prompted us to integrate the 3-D resistivity model. We explored the resistivity values at the bottom of the direct sample coring sites. Figure 2a shows the resistivity values at the closest SkyTEM soundings (average distance = 8.7 m; maximum distance = 19.4 m) at a depth that corresponds to the bottom of the field coring locations. From the plot, we notice that resistivities recorded at the 14 locations are rather variable both within and between sites: they are generally lower at Site 1 (blue dots) than at Site 2 (red dots). One of the 14 points falls more than 1.5 times the interquartile range above the third quartile (orange lines in Figure 2a); hence, it can be considered an outlier and will be excluded from our analyses.

A leave-one-out procedure was then used to calculate the accuracy of the ANN prediction ability. The cross-validation plot is visible in Figure 2b, where the 45° slope line is also plotted for reference as dotted line. From the plot we notice that most of the peat thickness values are well predicted by the ANN, and this is valid also for the 28 no peat points (green dots in Figure 2b) that fall very close to zero a part for two points where the ANN predicts 1.3 m and 2.8 m instead of zero peat thickness. Considering the location where we could not reach the peat bottom due to the limitations of our auger length (maximum 8.5 m), we notice that the ANN predicts a 3.96-m thickness. In conclusion, we find that the ANN slightly underestimates peat thickness, with an average residual of −0.14 m and a root-mean-square error (RMSE) of 0.93 m. These values are calculated considering only the 13 field measurements where peat thickness is greater than 0. If we also include the additional 28 points where peat thickness is known to be 0, the average residual is 0.07 m, and the RMSE is 0.71 m.

Synthetic modeling, included in the supporting information, clearly shows that had the substrate been more conductive (e.g., a thick clay layer), as it often is the case in peatlands in other parts of the world (Comas et al., 2015), the peat bottom would have been delineated by the AEM alone, with no need of using an ANN and constrain it based on boreholes. However, we speculate that since the ANN addresses the issue of spatial variability of threshold resistivity, too, not just the issue of poor resistivity contrast, the ANN would still enhance the interpretation of peat thickness even where there is a more conductive substrate.

After determining the accuracy of the ANN in predicting the thickness at the measuring points, we now discuss its accuracy in determining the horizontal extension of peatlands. Figure 3 shows the map of the SkyTEM sounding points falling within the 19 km^2 study area and colored based on the peat thickness retrieved with the ANN method. We notice that there is a good qualitative correspondence with the areas present in the NIBIO map (green polygons in Figure 3) especially in the southern part of the study area.

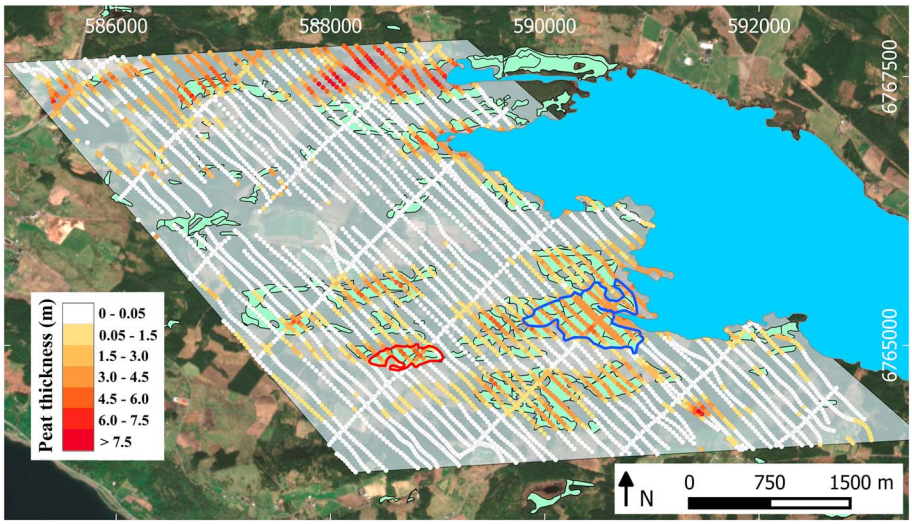

Figure 3. Map of the peatlands obtained with the artificial neural network. Green polygons are wetland outlines from the NIBIO map, while the large light blue polygon is the lake. (Coordinate reference system: WGS 84 UTM 32N. Base map has been produced from a Sentinel-2 image.)

The territories in the northeast that are erroneously classified as peatlands by the system correspond to a large estuary possibly characterized by wet soils. Those in the northwest are located across the small river that forms the same estuary.

In order to quantitatively test the accuracy of the peatlands map, we produce a confusion matrix with the sounding points with thickness larger than 0.05 m that we consider "peatland" versus the peatland areas extracted from the NIBIO Institute map (Table S4 in the supporting information).

In total we have 4,635 sounding points within the study area. We notice that out of the 712 sounding points that should have been classified as peatland based on the NIBIO map, 558 were correctly allocated (that corresponds to 78%), while 154 points were classified as "nonpeatland" (22%). Looking at the 3,923 soundings falling in the areas outside the peatlands, 1,201 points were erroneously classified peatland, which corresponds to the 30.6% of the total, while 2,722 points were correctly allocated as nonpeatland (69.4 %). The overall accuracy of the classification is 71%. The Cohen's k coefficient is 0.3, suggesting that even if the overall accuracy obtained with the classification is acceptable, some soundings were correctly classified by chance.

The peatland extension and thickness retrieved with this methodology allow one to estimate the volume of peat stored in a specific site and therefore to estimate its total organic carbon content. In order to extract this information, first we interpolate using the ordinary kriging the soil elevation and the peat bottom values retrieved at the SkyTEM sounding points in order to extract the two surfaces, and then we subtract the second from the first to calculate the total peat volume across the two study sites. We estimate that study Site 1 stores 1,218,482 m^3 of peat, and considering that the average OCC by soil volume that we determined equals 0.028 g/cm^3, based on our calculations, Site 1 contains 34 kt of organic carbon. Study Site 2 stores 291,035 m^3 of peat with an average OCC by soil volume of 0.023 g/cm^3, for a total 6.7 kt of organic carbon. As for the uncertainty associated with these estimates, the largest contribution is due to the systematic underestimation of peat depth (i.e., −0.14 m) that propagates into the volume calculation of the peat, which corresponds to −4.1% for Site 1 and −4.9% for Site 2. Therefore, at Site 1 we underestimate the organic carbon content by 1.4 kt, while at Site 2 the underestimation error is 0.3 kt.

5. Conclusions

Conservation actions targeted at avoiding potential greenhouse gas emissions from peatlands require accurate assessment of the carbon stored in peatlands at the regional to the global scale, and hence, a reliable method to quantify peat thickness and volume is essential. However, despite their importance, the

accurate quantification of peatlands extension and volume is still lacking. Airborne Electromagnetic has been used in this study to determine the presence, thickness and extension of peat deposits in a Norwegian territory rich in wetlands. We found that peat resistivity of bogs is variable, increasing from the surface to the bottom of the bogs in the range 140–380 Ω·m. Despite peat deposits are often located over clay (which is characterized by extremely low resistivities), in this study the AEM did not detect any significant conductive strata indicative of clay layers underneath the peats. On the contrary, the resistivity of the bottom layers has been found to be higher than the resistivity of the peat, corresponding to bedrock or moraine material. If an underlying layer of clay was present, as suggested by some samples collected during the field survey, we speculate it was too thin to be detected by the AEM system. However, further inspections are needed to confirm this hypothesis. The lack of low resistivity layer that separates the peat deposits from the deep geological structures strongly limited the effectiveness of AEM in accurately determining the peat thickness on its own. Moreover, the resistivity of the peat-substrate interface was spatially variable. To overcome these limitations, we used an ANN constrained with the thickness measurements of the peat from direct boreholes sampling to simulate peat depth and extension. The accuracy obtained in determining the peat thickness was tested against independent measurements, performing a leave-one-out analysis. The resulted average residual is −0.14 m, with RMSE of 0.93 m, which we consider acceptable if compared to the average peat thickness measured in the area which equals to 3.64 m. The methodology allowed us to also map the distribution of peatlands across the entire 19 km^2 study area. We found a good agreement of the produced map with the reference map provided by NIBIO, even though our methodology overestimated the presence of peatlands within the study area, especially in its north part where an estuary was mistakenly classified as peatland. The limited amount of field data used to train and validate the peatland model probably represented the main limit in the detection of the peat volume. Overall, final results allowed us to calculate the volume of the peat deposits and the organic carbon content, showing that AEM data can be successfully used to study peatlands at the regional scale and retrieve the organic carbon pool. We expect the performance of AEM to peat volume mapping to increase significantly in presence of a conductive substratum (see supporting information for simulation results that support this conclusion). We also expect this methodology to be effective in other situations and regions of the world. The main obstacles may be the high cost of the AEM surveys, the presence of infrastructures that interfere with the AEM signal, and the limited number of field measurements that is feasible to collect over large territories. Another limit may arise in quantifying the carbon content in sites showing markedly different levels of peat decomposition/soil organic matter content throughout the soil profile. In those cases AEM may not provide high enough vertical and horizontal spatial resolutions to properly link the variability of soil properties to electrical conductivity.

Acknowledgments
This research is part of the project CReScenDo (Combining Remote Sensing Technologies for Peatland Detection and Characterization) that has received funding from the European Union's Horizon 2020 research and innovation program under the Marie Skłodowska-Curie grant agreement 747809. Data used for this paper are freely available through OpenAIRE/Zenodo at http://doi.org/10.5281/zenodo.3238632. We thank the National Norwegian Railroad Authorities for having kindly provided the SkyTEM data that were collected as part of the InterCity Project. We also thank Arne Grønlund and Knut Bjørkelo of the Norwegian Institute of Bioeconomy Research for having provided the map of the distribution of peatlands in the study area. This research would have not been possible without the precious help of Anita, Emma, and Marco, who gave a fundamental support with the field survey. Comments from Valeriy Ivanov, Lee Slater, Neal J. Pastick, and anonymous reviewers have greatly improved the clarity of this paper.

References

Aarhus GeoSoftware (2018). Aarhus Workbench. Retrieved from https://www.aarhusgeosoftware.dk/ (accessed on 22 March 2018).

Ballhorn, U., Jubanski, J., & Siegert, F. (2011). ICESat/GLAS data as a measurement tool for peatland topography and peat swamp forest biomass in Kalimantan, Indonesia. *Remote Sensing*, *3*(9), 1957–1982. https://doi.org/10.3390/rs3091957

Ballhorn, U., Siegert, F., Mason, M., & Limin, S. (2009). Derivation of burn scar depths and estimation of carbon emissions with LIDAR in Indonesian peatlands. *Proceedings of the National Academy of Sciences of the United States of America*, *106*(50), 21,213–21,218. https://doi.org/10.1073/pnas.0906457106

Boon D., Kessler H., Raines M., Kuras O., Auton C., Williams J., et al. (2008). Modelling Scottish peat stratigraphy using integrated electrical geophysics. [Lecture] In: Reinforced water: Engineering and environmental considerations in construction over peat, Edinburgh, Scotland, 11 March 2008. http://nora.nerc.ac.uk/id/eprint/4830/

Comas, X., & Slater, L. (2004). Low-frequency electrical properties of peat. *Water Resources Research*, *40*, W12414. https://doi.org/10.1029/2004WR003534

Comas, X., Terry, N., Slater, L., Warren, M., Kolka, R., Kristiyono, A., et al. (2015). Imaging tropical peatlands in Indonesia using ground-penetrating radar (GPR) and electrical resistivity imaging (ERI): Implications for carbon stock estimates and peat soil characterization. *Biogeosciences*, *12*(10), 2995–3007. https://doi.org/10.5194/bg-12-2995-2015

Draper, F. C., Roucoux, K. H., Lawson, I. T., Mitchard, E. T. A., Coronado, E. N. H., Lahteenoja, O., et al. (2014). The distribution and amount of carbon in the largest peatland complex in Amazonia. *Environmental Research Letters*, *9*(12), 124017. https://doi.org/10.1088/1748-9326/9/12/124017

Elijah, A. A., Folorunso, A., & Olubunmi, J. (2012). An application of 2D electrical resistivity tomography in geotechnical investigations of foundation defects: A case study. *Journal of Geology and Mining Research*, *3*(12), 142–151. https://doi.org/10.5897/JGMR12.002

Intergovernmental Panel on Climate Change (2014). Climate change 2014: Mitigation of climate change. Contribution of Working Group III to the Fifth Assessment Report of the Intergovernmental Panel on Climate Change [Edenhofer, O. et al.]. Cambridge University Press, Cambridge, United Kingdom and New York, NY, USA.

Jaenicke, J., Rieley, J. O., Mott, C., Kimman, P., & Siegert, F. (2008). Determination of the amount of carbon stored in Indonesian peatlands. *Geoderma*, *147*(3-4), 151–158. https://doi.org/10.1016/j.geoderma.2008.08.008

Joosten, H. (2010). *The global peatland CO2 picture: Peatland status and drainage related emissions in all countries of the world* (p. 36). Wageningen, Netherlands: Wetlands International.

Kowalczyk, S., Żukowska, K. A., Mendecki, M. J., & Łukasiak, D. (2017). Application of electrical resistivity imaging (ERI) for the assessment of peat properties: A case study of the Całowanie Fen, Central Poland. *Acta Geophysica*, *65*(1), 223–235. https://doi.org/10.1007/s11600-017-0018-9

Nelson, D. W., & Sommers, L. E. (1996). Total carbon, organic carbon, and organic matter. In A. L. Page et al. (Eds.), *Methods of Soil Analysis. Part 2*, *Agronomy Series No. 9, ASA SSSA* (2nd ed., Chap. 29, pp. 539–577). Madison.

Norwegian Geotechnical Institute (2015). InterCity prosjekt: Helikopterbasert AEM Brumunddal-Lillehammer, datarapport. (In Norwegian).

Page, S. E., Siegert, F., Rieley, J. O., Boehm, H. V., Jaya, A., & Limin, S. (2002). The amount of carbon released from peat and forest fires in Indonesia during 1997. *Nature*, *420*(6911), 61–65. https://doi.org/10.1038/nature01131

Parry, L. E., West, L. J., Holden, J., & Chapman, P. J. (2014). Evaluating approaches for estimating peat depth. *Journal of Geophysical Research: Biogeosciences*, *119*, 567–576. https://doi.org/10.1002/2013JG002411

Pfaffhuber, A. A., Bazin, S., Kasin, K., Anschütz, H., Sandven, R., Montafia, A., et al. (2016). In situ detection of sensitive clays from a geophysical perspective. In B. M. Lehane, et al. (Eds.), *5th International Conference on Geotechnical and Geophysical Site Characterisation (ISC5)*, (pp. 917–922). Australia: Gold Coast.

Puranen, R., Saavuori, H., Sahala, L., Suppala, I., Makila, M., & Lerssi, J. (1999). Airborne electromagnetic mapping of surficial deposits in Finland. *First Break*, *17*(5), 145–154. https://doi.org/10.1046/j.1365-2397.1999.00704.x

Rudiyanto, M. B., Setiawan, B. I., Saptomo, S. K., & McBratney, A. B. (2018). Open digital mapping as a cost-effective method for mapping peat thickness and assessing the carbon stock of tropical peatlands. *Geoderma*, *313*, 25–40. https://doi.org/10.1016/j.geoderma.2017.10.018

Schamper, C., Auken, E., & Sørensen, K. (2014). Coil response inversion for very early time modelling of helicopter-borne time-domain electromagnetic data and mapping of near-surface geological layers. *Geophysical Prospecting*, *62*(3), 658–674. https://doi.org/10.1111/1365-2478.12104

Skurdal, G. H., Pfaffhyber, A. A., Davis, A., Bazin, S., Nyboe, N. S., & Foged, N. (2018). Applying system response to improve the near-surface resolution of AEM models. AEM2018—International Workshop on Airborne Electromagnetics, June 17-20 2018, Kolding, Denmark.

Slater, L. D., & Reeve, A. (2002). Investigating peatland stratigraphy and hydrogeology using integrated electrical geophysics. *Geophysics*, *67*(2), 365–378. https://doi.org/10.1190/1.1468597

Turetsky, M. R., Benscoter, B., Page, S., Rein, G., van der Werf, G. R., & Watts, A. (2015). Global vulnerability of peatlands to fire and carbon loss. *Nature Geoscience*, *8*(1), 11–14. https://doi.org/10.1038/NGEO2325

Viezzoli, A., Christiansen, A. V., Auken, E., & Sørensen, K. I. (2008). Quasi-3D modeling of airborne TEM data by spatially constrained inversion. *Geophysics*, *73*(3), F105–F113. https://doi.org/10.1190/1.2895521

Vignoli, G., Sapia, V., Menghini, A., & Viezzoli, A. (2017). Examples of improved inversion of different airborne electromagnetic datasets via sharp regularization. *Journal of Environmental and Engineering Geophysics*, *22*(1), 51–61. https://doi.org/10.2113/JEEG22.1.51

Warner, B. G., Nobes, D. C., & Theimer, B. D. (1990). An application of ground penetrating radar to peat stratigraphy of Ellice Swamp, southwestern Ontario. *Canadian Journal of Earth Sciences*, *27*(7), 932–938. https://doi.org/10.1139/e90-096

References From the Supporting Information

Auken, E., Breiner, M., Nebel, L., Pellerin, L., Thomsen, P., & Srensen, K. I. (2001). EMMA-Electromagnetic modelling and analysis. EEGS Birmingham Proceedings. Anonymous. Anonymous. Birmingham, UK: EEGS. 114–115, 2001. JED.

Auken, E., & Christiansen, A. V. (2004). Layered and laterally constrained 2D inversion of resistivity data. *Geophysics*, *69*(3), 752–761. https://doi.org/10.1190/1.1759461

Kirkegaard, C., & Auken, E. (2015). A parallel, scalable and memory efficient inversion code for very large scale airborne EM surveys. *Geophysical Prospecting*, *63*(2), 495–507. https://doi.org/10.1111/1365-2478.12200

Viezzoli, A., Kaminski, V., & Fiandaca, G. (2017). Modeling induced polarization effects in helicopter TEM data: Synthetic case studies. (82-2) E31–E50 Geophysics.